SORET AND DUFOUR EFFECTS ON CHEMICALLY REACTING AND VISCOUS DISSIPATING NANOFLUID FLOWING PAST A MOVING POROUS PLATE IN THE PRESENCE OF A HEAT SOURCE/SINK

Aastha AASTHA*⊙, Khem CHAND*⊙

*Department of Mathematics and Statistics, Himachal Pradesh University, Summer Hill, Shimla-171005, India

aastha2101@gmail.com, khemthakur99@gmail.com

Abstract: This study performed a numerical investigation of the Soret and Dufour effects on unsteady free convective chemically reacting nanofluid flowing past a vertically moving porous plate in the presence of viscous dissipation and a heat source/sink. The equations directing the flow are non-dimensionalised, modified to ordinary differential equations and emerging equations are resolved computationally by using the bvp4c function in MATLAB software. The results obtained from this analysis indicate that the resulting velocity of the nanofluid increases with increasing Grashof number, mass Grashof number and porosity parameter. An increase in the Dufour number increases the fluid temperature, whereas the concentration profile declines with the increase in the Schmidt number. It is also observed that the skin friction coefficient, Nusselt number and Sherwood number increase with increasing magnetic field parameter, Eckert number and Schmidt number, respectively. The present study reveals the impact of Soret and Dufour effects on heat and mass transfer rates in chemically reacting and viscous dissipating nanofluids.

Keywords: Soret and Dufour effects, viscous dissipation, heat source/sink, chemically reacting nanofluid, free convection

1. INTRODUCTION

The heat transfer characteristics of fluids are used in all heat transfer applications. Well-known conventional heat transfer fluids are water, ethylene glycol and propylene glycol. Numerous investigations have been carried out to improve the poor heat transfer properties of these fluids. A novel method adopted to enhance their properties is formulation of nanofluids. Nanofluids are manufactured by mixing base fluid having low thermal conductivity with solid nanoparticles having high thermal conductivity, and consequently, the new fluid, i.e., nanofluid, is formed, which has a higher heat transfer characteristic than the base fluid. In addition, nanofluids contain nanometer-sized particles, which are prepared by colloidal suspension of nanoparticles in heat transfer fluids such as water, oil, diesel, ethylene and glycol. Nanoparticles used in nanofluids are generally made of metals, oxides, carbides or carbon nanotubes. Nanofluids have enhanced thermophysical properties like thermal conductivity, specific heat, viscosity and convective heat transfer in comparison to base fluids. These thermophysical properties of nanofluids are still under exploration and needs to be further elaborated. The thermophysical properties of nanofluids and the elements that can reform these properties were investigated by Gupta et al. [1]. The found that the main factors influencing these properties are shape, size, material, concentration and temperature of nanoparticles, together with the base fluid. Nanofluids have a wide range of advantages such as high specific surface area and thus more heat transfer surface between the particles and fluids, high dispersion stability with predominant Brownian motion of particles, reduced pumping power as compared to pure liquid to achieve equivalent heat

transfer intensification, and reduced particle clogging as compared to conventional slurries, thus promoting miniaturisation. The characteristic features of high thermal conductivities and heat transfer coefficients in comparison to those of conventional fluids make nanofluids suitable for the subsequent generation of flow and heat transfer fluids. Nanofluids have attracted the attention of many physicists, chemists and engineers around the world. Turkyilmazoglu and Pop [2] analysed the heat and mass transfer characteristics of some nanofluids flowing past a vertical infinite flat plate and the radiation effect for two distinct types of thermal boundary conditions. Dalir and Nourazar [3] found out the boundary layer flow of various nanofluids flowing past a moving semi-infinite plate using the homotopy perturbation method. Ghalambaz et al. [4] found the numerical solution for the natural convective flow of nanofluids over a convectively heated vertical plate in a saturated Darcy porous medium. Sulochana et al. [5] addressed the unsteady magnetohydrodynamic boundary layer flow of a nanofluid flowing past a permeable stretching surface sheet immersed in a porous medium. Mishra et al. [6] carried out a numerical study of an oscillatory unsteady Magnetohydrodynamic flow, heat and mass transfer in a vertical rotating channel with an inclined uniform magnetic field and hall effect. Ashwinkumar et al. [7] determined the momentum, heat and mass transfer characteristics of a magnetic nanofluid flowing past a vertical plate embedded in a porous medium filled with ferrous nanoparticles. Samrat et al. [8] found the heat and mass transfer characteristics of an unsteady flow of Casson nanofluid flowing past an elongated surface with a thermal radiation effect. Shaw et al. [9] formulated the transfer of mass and heat of nanofluid flowing over three different geometries of a non-Darcy permeable vertical

sciendo

Aastha Aastha, Khem Chand
Soret and Dufour Effects on Chemically Reacting and Viscous Dissipating Nanofluid Flowing Past a Moving Porous Plate in the Presence of a Heat Source/Sink

DOI 10.2478/ama-2023-0030

cone/wedge/vertical plate under viscous dissipation and thermal radiation. The Soret, Dufour, hall current and rotation effects on MHD natural convective heat and mass transfer flow past an accelerated vertical plate through a porous medium were calculated by Kumar et al. [10]. Khan et al. [11] scrutinised the magnetohydrodynamic flow of nanomaterials over a stretchable surface with melting heat effect, dissipation, heat flux, Joule heating effect, thermophoresis, Brownian motion and entropy generation. Rasheed et al. [12] discussed the impact of nanofluid flowing over an elongated moving surface with a uniform hydromagnetic field and non-linear heat reservoir. Kumawat et al. [13] analysed the entropy generation of MHD blood flowing through a stenosed permeable curved artery with a heat source and chemical reaction. Tlili et al. [14] studied the effect of fibre laser welding parameters on temperature distribution, weld bead dimensions, melt flow velocity and microstructure by using finite volume and experimental methods. Hejazi et al. [15] explored the role of velocity slip effects for mixed convection flow of nanofluid due to an inclined surface. Anantha Kumar et al. [16] studied the control of electromagnetic induction over the flow and heat transmission in shear-thickening hybrid nano- and ferrofluids for cooling/heating applications. Veera Krishna et al. [17] studied the effect of thermal conductivity on temperature on free convective movement of an incompressible viscous fluid through a heated uniform and vertical wavy surface. Khanduri et al. [18] focussed on the effect of Hall and ion slips on MHD blood flowing through a catheterised multi-stenosis artery with thrombosis. Sharma et al. [19] analysed the higher order endothermic/exothermic chemical reactions with activation energy by considering thermophoresis and Brownian motion effects on MHD mixed convective flow across a vertical stretching surface. The entropy optimisation of MHD flow past a continuously stretching surface was carried out by Khanduri et al. [20].

After reviewing the aforementioned research studied, we analysed the free convective flow with heat and mass transfer of a heat-generating and chemically reacting nanofluid passing through a vertical moving porous plate in a conducting field taking into account the viscous dissipation effect along with Soret and Dufour effects. To the best of our knowledge, no study has focussed on the chemical reaction, heat source/sink and viscous dissipation effects on MHD flow of a nanofluid passing through a vertically infinite moving porous plate subjected to Soret and Dufour effects. Therefore, to bridge this research gap and due to its realistic significance in the number of effective applications in geophysics and energy-related problems, we carried out this study. The study of heat and mass transfer rates of nanofluids as a combination of base fluid and low concentration of nano-sized particles of metals is noteworthy due to its wide spectrum of applications in engineering devices in power and chemical engineering, military, surveillance cameras, microchips and medicine for drug delivery, specifically for cancer cells. Continuing on this line of research, our aim is to solve the governing equations corresponding to the physical model under analysis with the help of the bvp4c numerical scheme and to identify effects of different flow parameters in the equations. For this, coupled non-linear partial differential equations are transformed to ordinary differential equations by the Laplace transform technique and then solved numerically by using the bvp4c function in MATLAB. The numerical results attained are explored using contour plots, and main research outcomes are mentioned at the end of this article.

2. MATHEMATICAL FORMULATION

In this research, a magneto-nano and heat-generating fluid flowing towards an infinite porous plate, which is oriented in vertical direction and moving with an impulsive motion as shown in Fig. 1, is considered.
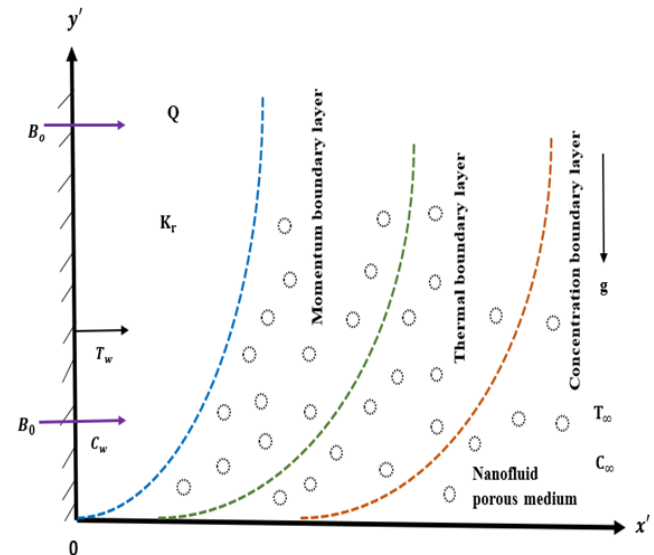

Fig 1. Physical configuration of the problem

We take into account an unsteady free convective, heat and mass transfer flow by incorporating Soret and Dufour effects along with viscous dissipation. The y' axis is vertically upwards along with the plate, while the x' axis is in a direction perpendicular to it. The magnetic field B_0, which is uniformly transverse, is applied parallel to the x' axis. The temperature of the plate fluctuated from T'_∞ to T'_w, and the concentration of the plate varied from C'_∞ to C'_w when the movement of the plate starts in its plane with velocity λu_0 at time $t' > 0$. Water with nanoparticles of copper (Cu) is taken as the base fluid, and both are in thermal equilibrium. In equations governing the flow of problem, density is considered to be linearly dependent on temperature. The magnetic field is supposed to be $\vec{B} \equiv (0, B_o, 0)$ because in comparison to the applied magnetic field, the induced magnetic field generated by the flow of fluid is considered negligible. Furthermore, we suppose the electric field as $\vec{E} = (0,0,0)$ to consider the effect of polarisation of the fluid negligible (Cramer et al. [21]). The basic equations of momentum, energy and concentration limited only to spherical nanoparticles governing the problem in the presence of magnetic field, thermal diffusion, heat source or sink, viscous dissipation, chemical reaction and Soret and Dufour effects are given as follows [22]:

$$\rho_{nf} \frac{\partial u'}{\partial t'} = \mu_{nf} \frac{\partial^2 u'}{\partial x'^2} + g(\rho\beta)_{nf}(T' - T'_\infty)$$
$$+ g(\rho\beta')_{nf}(C' - C'_\infty) - \sigma_{nf}B_o^2 u' - \frac{\mu_{nf}}{K'_p} u' \qquad (1)$$

$$(\rho C_p)_{nf} \frac{\partial T'}{\partial t'} = k_{nf} \frac{\partial^2 T'}{\partial x'^2} + \mu_{nf} \left(\frac{\partial u}{\partial x'}\right)^2 + D\rho_{nf}C_p \frac{\partial^2 C'}{\partial x'^2} + q_0(T' - T'_\infty) \qquad (2)$$

$$\frac{\partial C'}{\partial t'} = D \frac{\partial^2 C'}{\partial x'^2} + D_1 \frac{\partial^2 T'}{\partial x'^2} + K_1(C' - C'_\infty) \qquad (3)$$

The thermal conductivity of nanofluid is given as follows:

$$k_{nf} = k_f \left[\frac{k_s + 2k_f - 2\phi(k_f - k_s)}{k_s + 2k_f + \phi(k_f - k_s)} \right] \qquad (4)$$

Also,

$$\mu_{nf} = \frac{\mu_f}{(1-\phi)^{2.5}}, \rho_{nf} = (1-\phi)\rho_f + \phi\rho_s,$$
$$(\rho C_p)_{nf} = (1-\phi)(\rho C_p)_f + \phi(\rho C_p)_s$$
$$(\rho\beta)_{nf} = (1-\phi)(\rho\beta)_f + \phi(\rho\beta)_s$$
$$(\rho\beta')_{nf} = (1-\phi)(\rho\beta')_f + \phi(\rho\beta')_s$$
$$\sigma_{nf} = \sigma_f \left[1 + \frac{3(\sigma-1)}{(\sigma+2)-(\sigma-1)\phi} \right], \sigma = \sigma_s/\sigma_f \qquad (5)$$

where *nf*, *f* and *s* in Eqs. (1)–(5) indicate thermophysical properties of the nanofluid, base fluid and the nanoparticles, respectively.

The corresponding initial and boundary conditions are given as follows:

$$u' = 0, T' = T'_\infty, C' = C'_\infty \text{ for all } x' \geq 0 \text{ and } t' = 0$$
$$u' = \lambda u_o, T' = T'_w, C' = C'_w \text{ at } x' = 0 \text{ and } t' > 0$$
$$u' \to 0, T' \to T'_\infty, C' \to C'_\infty \text{ as } x' \to \infty \text{ and } t' > 0 \qquad (6)$$

where $\lambda = 0$ signifies the direction of the moving plate when the plate is at rest, while $\lambda = \pm 1$ indicates the direction of the plate moving in both forward and backward directions.

Using the non-dimensional variables in Eqs. (1)–(3),

$$x = \frac{u_0 x'}{v_f}, t = \frac{u_0^2 t'}{v_f}, u = \frac{u'}{u_0}, \theta = \frac{T'-T'_\infty}{T'_w - T'_\infty}, C = \frac{C'-C'_\infty}{C'_w - C'_\infty},$$
$$K'_P = \frac{K v_{nf}^2}{u_0^2}$$

The governing equations in the non-dimensional form are as given follows:

$$\frac{\partial u}{\partial t} = \frac{\partial^2 u}{\partial x^2} + Gr\, A_2\theta + Gc\, A_5 C - M^2 A_3 u - \frac{1}{K}u \qquad (7)$$

$$\frac{\partial \theta}{\partial t} = \frac{1}{Pr}\frac{\partial^2 \theta}{\partial x^2} + Ec\left(\frac{\partial u}{\partial x}\right)^2 + Du\frac{\partial^2 C}{\partial x^2} + \frac{v}{Pr}Q\,\theta \qquad (8)$$

$$\frac{\partial C}{\partial t} = \frac{1}{S_c}\frac{\partial^2 C}{\partial x^2} + S_o\frac{\partial^2 \theta}{\partial x^2} + K_r C \qquad (9)$$

Where:

$$Gr(\text{Grashof number}) = \frac{g\beta_f \mu_f (T'_w - T'_\infty)}{u_0^3},$$

$$Gc(\text{mass Grashof number}) = \frac{g\beta_f^* \mu_f (C'_w - C'_\infty)}{u_0^3},$$

$$M^2(\text{magnetic parameter}) = \frac{\sigma_f B_0^2 v_f}{\rho_f u_0^2},$$

$$K(\text{porosity parameter}) = \frac{K'_p u_0^2}{v_f^2},$$

$$Pr(\text{Prandtl number}) = \frac{\mu_f C_p}{k_f},$$

$$Ec(\text{Eckert number}) = \frac{u_0^2}{C_p(T'_w - T'_\infty)},$$

$$Du(\text{Dufour number}) = \frac{D}{v_f}\left(\frac{C'_w - C'_\infty}{T'_w - T'_\infty}\right),$$

$$Q(\text{heat source/sink parameter}) = \frac{q_0 v_f^2}{k_f u_0^2},$$

$$S_c(\text{Schmidt number}) = \frac{v_f}{D},$$

$$S_o(\text{Soret number}) = \frac{D_1}{v_f}\left(\frac{T'_w - T'_\infty}{C'_w - C'_\infty}\right),$$

$$Kr(\text{Chemical reaction parameter}) = \frac{K_1 v_f}{u_0^2}$$

A_2, A_3 and A_5 are constants defined as follows:

$$A_2 = \left[\frac{(1-\phi)}{\rho_{nf}} + \frac{\phi(\rho\beta)_s}{(\rho\beta)_f \rho_{nf}} \right]$$

$$A_3 = \frac{\left[1 + \frac{3(\sigma-1)}{(\sigma+2)-(\sigma-1)\phi} \right]}{\left[\left(1 - \phi + \phi\frac{\rho_s}{\rho_f} \right) \right]}$$

$$A_5 = \left[\frac{(1-\phi)}{\rho_{nf}} + \frac{\phi(\rho\beta^*)_s}{(\rho\beta^*)_f \rho_{nf}} \right]$$

On application of the Laplace Transform technique, Eqs. (7)–(9) are transformed to the following forms of ordinary differential equations:

$$\frac{d^2\bar{u}}{dx^2} - \left(s + M^2 A_3 + \frac{1}{K} \right)\bar{u} + Gr\, A_2\bar{\theta} + Gc\, A_5\bar{C} = 0 \qquad (10)$$

$$\frac{1}{Pr}\frac{d^2\bar{\theta}}{dx^2} + Du\frac{d^2\bar{C}}{dx^2} + Ec\left(\frac{d\bar{u}}{dx}\right)^2 + \frac{v}{Pr}Q\bar{\theta} - s\bar{\theta} = 0 \qquad (11)$$

$$\frac{1}{S_c}\frac{d^2\bar{C}}{dx^2} + S_o\frac{d^2\bar{\theta}}{dx^2} - (s - Kr)\bar{C} = 0 \qquad (12)$$

as in Eqs. (10)–(12) is a complex parameter also known as Laplace operator, which is the same for all the equations.

The corresponding initial and boundary conditions in the non-dimensional form are given as follows:

$$t = 0: u = 0, \theta = 0, C = 0 \text{ for all } x \geq 0$$
$$t > 0: u = \lambda, \theta = 1, C = 1 \text{ at } x = 0$$
$$t > 0: u \to 0, \theta \to 0, C \to 0 \text{ as } x \to \infty \qquad (13)$$

2.1. Numerical solution

Due to the difficulty in finding exact solutions of non-linear partial differential Eqs. (7)–(9), the equations after transformation to ordinary differential equations (10–12) are numerically solved using the bvp4c function by MATLAB software. bvp4c is a method for obtaining numerical solution to the boundary value problems. The basic solution method is subjected to polynomial collocation with four Lobatto points for bvp4c. It uses the three-stage Lobatto IIIa formula. It is a collocation formula, and the collocation polynomial provides a solution that is accurate up to fourth order on a given interval. Before using bvp4c for solving a problem, we rewrite the given second or higher order ODEs as a system of first-order ODEs, which in the present problem in the following manner:

$\bar{\theta} = y(1)$	$\bar{C} = y(3)$	$\bar{u} = y(5)$
$\bar{\theta}' = y(2)$	$\overline{C}' = y(4)$	$\bar{u}' = y(6)$

The approach is using to obtain parameterised initial conditions at the initial point of the interval. A standard ODE solver is used for arriving at the solution across the domain. After this, root finding is adopted to find the appropriate parameter values to apply the boundary conditions at the end point of the interval, which are then used for finding the solution across the domain. Hence, it is clear that the solver for initial value problems is turned into a solver for boundary value problems. This is the overall working algorithm for this numerical technique. The code used for this analysis is given in the appendix.

sciendo

Aastha Aastha, Khem Chand   DOI 10.2478/ama-2023-0030
Soret and Dufour Effects on Chemically Reacting and Viscous Dissipating Nanofluid Flowing Past a Moving Porous Plate in the Presence of a Heat Source/Sink

3. RESULT AND DISCUSSIONS

The follow-up of present investigation is currently premeditated with the help of significant sketched graphical features. Several important features of heat-generating and chemically reacting nanofluid with viscous dissipation incorporating Soret and Dufour effects in a conducting field by varying strengths of Dufour number (Du), Soret number (S_o), Schmidt number (S_c), magnetic parameter (M^2), porosity parameter (K), Grashof number (G_r), mass Grashof number (G_c), chemical reaction parameter (Kr), Prandtl number (Pr), Eckert number (Ec) and heat source/sink parameter (Q) have been explored through contours, as shown in Figs. 2–12. The values of the parameters are chosen arbitrarily. The dashed line shows variation of the motion of the fluid for the plate moving in backward direction, i.e., $\lambda = -1$, while the solid line shows variation of the plate moving in forward direction, i.e., $\lambda = 1$.

3.1. Effect of variation of different parameters on velocity field

Figs. 2–5 depict the effect of various governing parameters on velocity of the fluid.
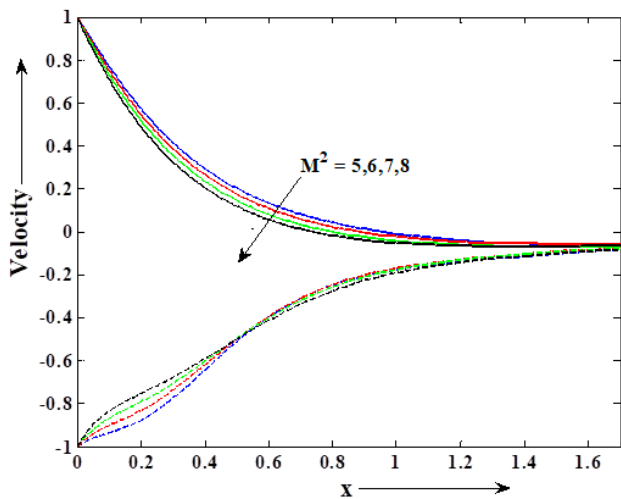

Fig. 2. Effect of M^2 on velocity when $Du = 5, S_o = 7, S_c = 2.5,$ $Ec = 0.08, K = 3, Gr = 4, Gc = 6, Pr = 1.9, R = 6,$ $Q = 4, Kr = 3$

The influence of the magnetic parameter (M^2) on velocity distribution is portrayed in Fig. 2. An electric charge is more violently pushed in contact with stronger magnetic field and from the regions of high magnetic field gradient. With an increase in the magnetic field strength, the velocity of nanofluid is found to decrease for motion of the plate in forward direction, while for motion of the plate in backward direction, velocity of the fluid first increases, and after a certain point of time, it starts reversing this trend. As there is a rise in resistive type of force called the Lorentz force, the influence of a transverse magnetic field on the conducting fluid has a tendency to slow down the motion of fluid in the boundary layer region. It produces more resistance to the phenomenon of transportation. The graphical representation of porosity parameter (K) on the velocity profile is depicted in Fig. 3. It is observed that

with growing K, velocity in the boundary layer increases with the motion of the plate in forward direction, and for backward motion, velocity first decreases and afterwards slightly increases. This is due to the fact that increasing the value of K assists the fluid considerably to move fast due to reduction in drag force. The porous material is the cause for restriction of flow of the fluid. Fig. 4 displays the effect of thermal Grashof number (Gr) on the velocity profiles. As the Grashof number increases, the velocity of the fluid increases for both forward and backward motions of the plate. For different values of the mass Grashof number (Gc), the velocity profile is plotted in Fig. 5. As the mass Grashof number increases, the velocity of the fluid increases for both forward and backward motions of the plate. This is due to the fact that an increase in the values of the thermal Grashof number and mass Grashof number has a tendency to increase thermal and mass buoyancy effects, which gives rise to an increase in the induced flow.
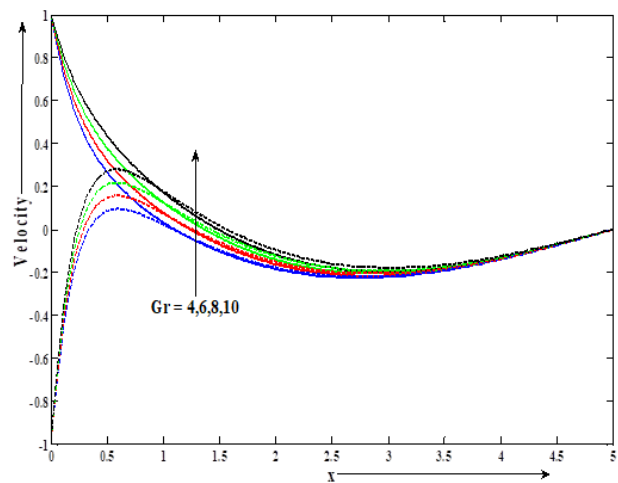

Fig. 4. Effect of Gr on velocity when $Du = 5, S_o = 7, S_c = 2.5,$ $Ec = 0.08, M^2 = 4, K = 0.7, Gc = 6, Pr = 1.9, R = 6,$ $Q = 4, Kr = 3$
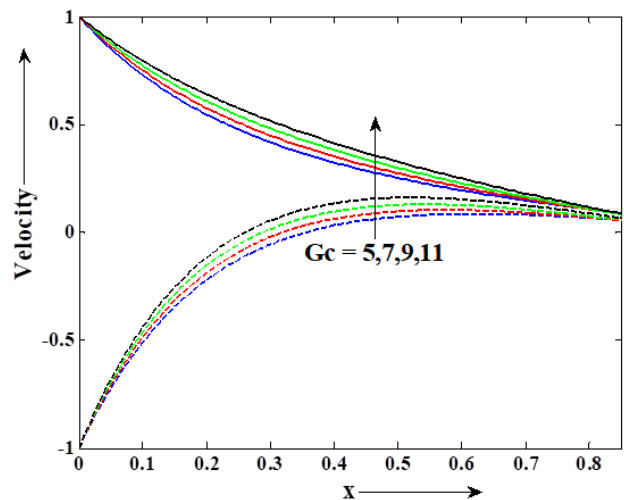

Fig. 5. Effect of Gc on velocity when $Du = 5, S_o = 7, S_c = 2.5,$ $Ec = 0.08, M^2 = 4, Gr = 4, K = 0.7, Pr = 1.9, R = 6,$ $Q = 4, Kr = 3$

3.2. Effect of variation of different parameters on skin friction

The values of skin friction (τ) for various parameters like thermal Grashof number (Gr), mass Grashof number (Gc), magnetic parameter (M^2) and porosity parameter (K) are given in Tabs. 1–4 ($R = 4$ taken as constant). It can be interpreted from Tabs. 1 and 2 that values of skin friction decrease with increasing values of Grashof number (Gr) and mass Grashof number (Gc). Table 3 shows the variation of skin friction with respect to the porosity parameter (K). Clearly, skin friction decreases with an increase in the values of the porosity parameter (K). The impact of magnetic parameter (M^2) on skin friction is evaluated and given in Table 4. Evidently, there is an increase in skin friction with increasing magnetic parameter. It also highlights a decrease in viscous drag forces.

Tab. 1. Variation with Grashof number

Gr	Gc	Du	S_o	S_c	Ec	M^2	K	Pr	Q	Kr	τ
5	6	2	4	0.44	1	9	0.5	0.79	4	0.5	2.9622
6	6	2	4	0.44	1	9	0.5	0.79	4	0.5	2.8326
7	6	2	4	0.44	1	9	0.5	0.79	4	0.5	2.7028
8	6	2	4	0.44	1	9	0.5	0.79	4	0.5	2.5729

Tab. 2. Variation with mass Grashof number

Gc	Gr	Du	S_o	S_c	Ec	M^2	K	Pr	Q	Kr	τ
6	5	2	4	0.44	1	9	0.5	0.79	4	0.5	2.9622
7	5	2	4	0.44	1	9	0.5	0.79	4	0.5	2.7850
8	5	2	4	0.44	1	9	0.5	0.79	4	0.5	2.6113
9	5	2	4	0.44	1	9	0.5	0.79	4	0.5	2.4406

Tab. 3. Variation with porosity parameter

K	Du	S_o	S_c	Ec	M^2	Gr	Gc	Pr	Q	Kr	τ
1.1	2	4	0.44	1	9	5	6	0.79	4	0.5	2.8198
1.3	2	4	0.44	1	9	5	6	0.79	4	0.5	2.8012
1.5	2	4	0.44	1	9	5	6	0.79	4	0.5	2.7875
1.7	2	4	0.44	1	9	5	6	0.79	4	0.5	2.7771

Tab. 4. Variation with magnetic parameter

M^2	Du	S_o	S_c	Ec	K	Gr	Gc	Pr	Q	Kr	τ
2	2	4	0.44	0.02	0.5	4	6	0.79	3	0.5	-0.4956
3	2	4	0.44	0.02	0.5	4	6	0.79	3	0.5	-0.0329
4	2	4	0.44	0.02	0.5	4	6	0.79	3	0.5	0.4994
5	2	4	0.44	0.02	0.5	4	6	0.79	3	0.5	1.0630

### 3.3. Effect of variation of different parameters on temperature field

Figs. 6–9 illustrate the effect of various governing parameters on temperature of the fluid. The low Eckert number ($Ec \ll 1$) allows making the judgement if the effects of self-heating due to dissipation can be overlooked or not. From Fig. 6, it can be concluded that the temperature of fluid decreases with increasing values of Eckert number (Ec), which shows a decrease in the thermal boundary layer thickness, thus consequently increasing the rate of heat transfer. Fig. 7 reveals that the temperature distribution profile of nanofluid decreases with increasing values of Prandtl number (Pr) predominantly due to a decrease in viscosity of the nanofluid. For a low Prandtl number (< 1), the thermal boundary layer is thicker than the velocity boundary layer. Fig. 8

depicts the effect of the heat source parameter (Q) on heat transfer processes. The heat source/sink parameter $Q > 0$ decreases the thermal conductivity, which results in the decrease in the temperature of the fluid.
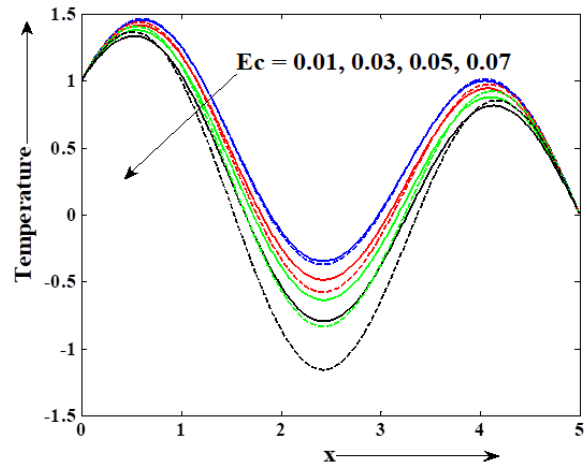
Fig. 6. Effect of Ec on temperature when Du = 5, $S_o = 2$, $M^2 = 9$, $K = 5$, $Gr = 4$, $Gc = 6$, $Pr = 0.76$, $R = 0.4$, $Q = 0.2$, $Kr = 5$, $S_c = 0.44$
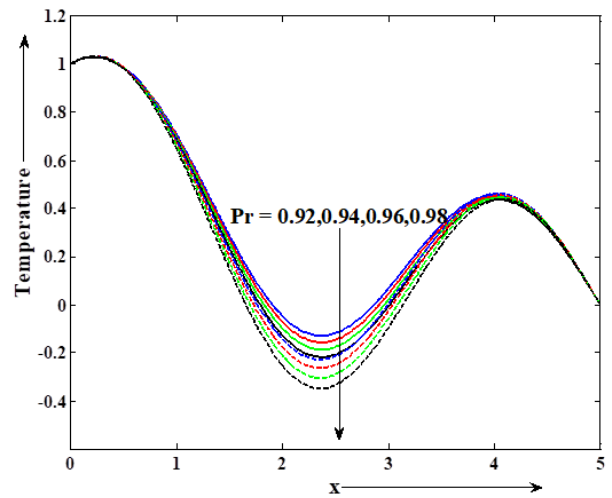
Fig. 7. Effect of Pr on temperature when Du = 7, $S_o = 2$, $M^2 = 9$, $K = 5$, $Gr = 4$, $Gc = 6$, $Ec = 0.07$, $R = 0.4$, $Q = 0.3$, $Kr = 5$, $S_c = 0.44$
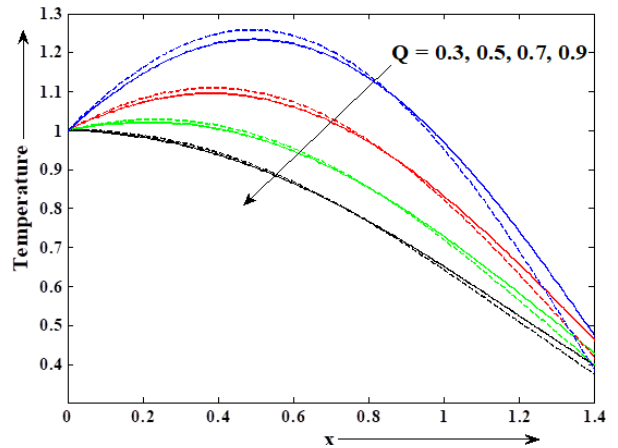
Fig. 8. Effect of Q on temperature when Du = 7, $S_o = 2$, $M^2 = 9$, $K = 5$, $Gr = 4$, $Gc = 6$, $Ec = 0.07$, $R = 0.4$, $Pr = 0.76$, $Kr = 5$, $S_c = 0.44$
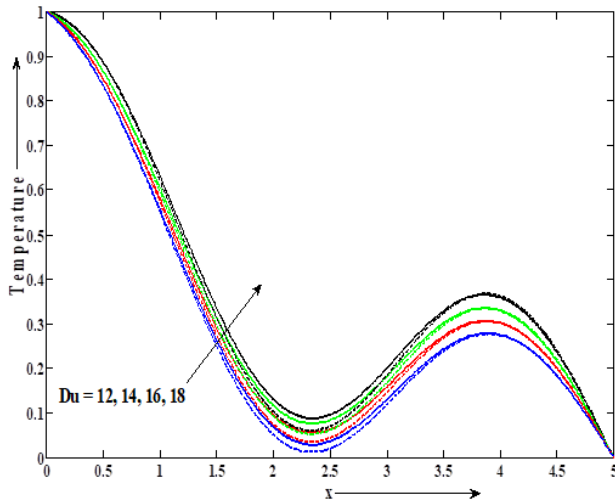
Fig. 9. Effect of Du on temperature when $Q = 0.3, S_o = 2,$ $M^2 = 9, K = 5, Gr = 4, Gc = 6, Ec = 0.07, R = 0.4,$ $Pr = 0.76, Kr = 5, S_c = 0.44$

Fig. 9 displays the variation in temperature with respect to Dufour number (Du). Higher values of the Dufour number causes an increase in temperature. It is clear from this graph that the temperature profile increases with an increase in the Dufour number (Du), which shows an increase in heat transfer.

3.4. Effect of variation of different parameters on Nusselt number coefficients

The variation in the Nusselt number with respect to the Prandtl number is measured and given in Tab. 5. From the table, it is seen that the Nusselt number increases with an increase in the Prandtl number. Tab. 6 shows the effect of the heat source/sink parameter (Q) on the Nusselt number. As the heat source parameter increases, the value of the Nusselt number also increases. Tab. 7 shows the variation in the Nusselt number with respect to the Eckert number. It was observed that the Nusselt number increases with an increase in the Eckert number (Ec). Tab. 8 shows the variation in the Nusselt number with an increase in the Dufour number (Du). It is found that the Nusselt number shows a decrease with the increasing values of the Dufour number $(R = 5$ taken as constant). It reflects an increase in the heat transfer rate.

Tab. 5. Variation with Prandtl number

Pr	Du	S_o	S_c	Ec	M^2	K	Gr	Gc	Q	Kr	Nu
0.82	2	6	0.57	0.04	9	1.5	5	6	4	2	3.2663
0.84	2	6	0.57	0.04	9	1.5	5	6	4	2	3.2757
0.86	2	6	0.57	0.04	9	1.5	5	6	4	2	3.2850
0.88	2	6	0.57	0.04	9	1.5	5	6	4	2	3.2942

Tab. 6. Variation with heat source parameter

Q	Du	S_o	S_c	Ec	M^2	K	Gr	Gc	Pr	Kr	Nu
1	2	6	0.57	0.04	9	0.5	5	6	0.82	5	0.8377
2	2	6	0.57	0.04	9	0.5	5	6	0.82	5	2.2000
3	2	6	0.57	0.04	9	0.5	5	6	0.82	5	2.8508
4	2	6	0.57	0.04	9	0.5	5	6	0.82	5	3.4073

Tab. 7. Variation with Eckert number

Ec	Du	S_o	S_c	Q	M^2	K	Gr	Gc	Pr	Kr	Nu
0.1	2	6	0.57	1	3	0.5	5	6	0.82	5	0.4686
0.2	2	6	0.57	1	3	0.5	5	6	0.82	5	0.7026
0.3	2	6	0.57	1	3	0.5	5	6	0.82	5	0.7532
0.4	2	6	0.57	1	3	0.5	5	6	0.82	5	0.8377

Tab. 8. Variation with Dufour number

Du	S_o	S_c	Q	M^2	K	Gr	Gc	Ec	Pr	Kr	Nu
5	6	0.57	1	3	0.5	5	6	0.02	0.82	5	0.8704
6	6	0.57	1	3	0.5	5	6	0.02	0.82	5	0.8649
7	6	0.57	1	3	0.5	5	6	0.02	0.82	5	0.8559
8	6	0.57	1	3	0.5	5	6	0.02	0.82	5	0.8402

3.5. Effect of variation in different parameters on concentration field

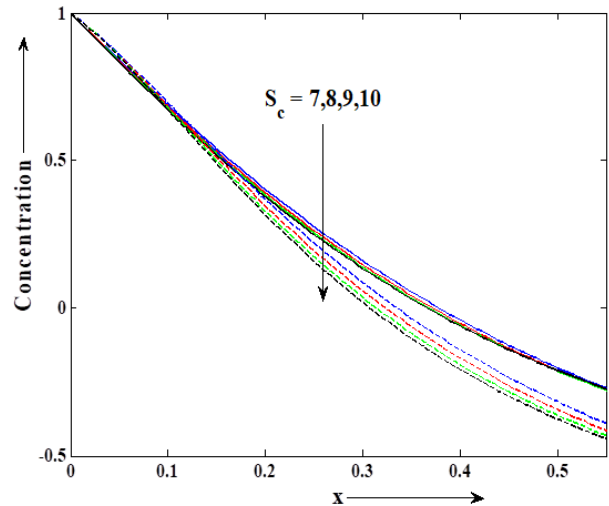Figs. 10–12 show the effect of various governing parameters on the concentration of fluid.

Fig. 10. Effect of S_c on concentration when $Du = 3, S_o = 4,$ $S_c = 3.5, Ec = 0.02, M^2 = 9, K = 2, Gr = 4, Gc = 6,$ $Pr = 0.79, R = 0.4, Q = 1, Kr = 5$
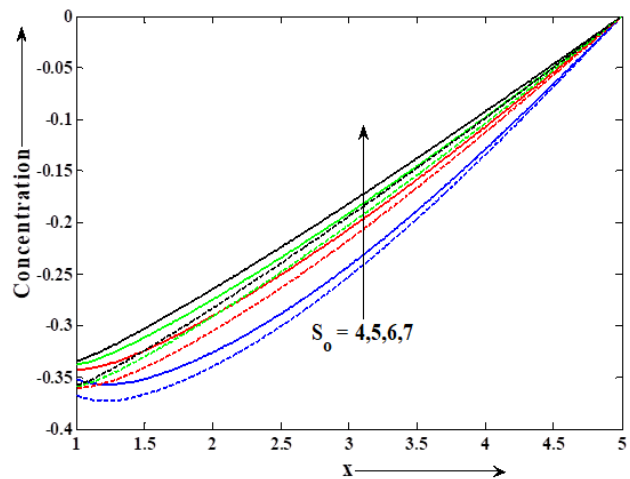

Fig. 11. Effect of S_0 on concentration when $Du = 2, S_c = 1.5,$ $Ec = 0.02, M^2 = 9, K = 0.5, Gr = 4, Gc = 6, Pr = 0.79,$ $R = 4, Q = 1, Kr = 5$
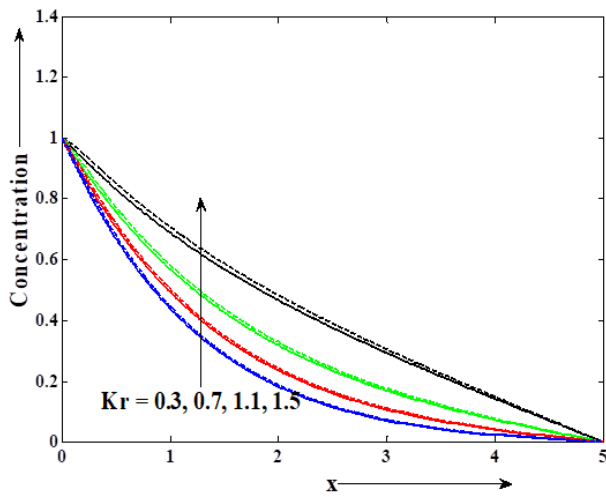
Fig. 12. Effect of Kr on concentration when $Du = 2, S_0 = 4$, $S_c = 0.44, Ec = 0.02, M^2 = 9, K = 0.5, Gr = 4, Gc = 6$, $Pr = 0.79, R = 4, Q = 1$

Fig. 10 depicts the variation in the concentration field subjected to Schmidt number (S_c). When the Schmidt number is high, the momentum is transported by molecular means across a liquid much more effectively than species. This figure reveals that an increase in S_c reduces the concentration profile. An increase in the Schmidt number results in weaker solute diffusivity, allowing a shallower penetration of the solutal effect. As a consequence, the concentration decreases with increasing S_c. From Fig. 11, it is evident that concentration profile increases with an increase in the Soret number (S_o). The higher values of the Soret number develops a higher convective flow. Fig. 12 describes the chemical reaction parameter (Kr) effect on nanofluid concentration profile. Small values of the chemical reaction parameter results in a decrease in the heat transfer coefficient and an increase in the mass transfer rate. As foreseen, the concentration increases with an increase in Kr. It reveals that with an increase in concentration under the influence of the chemical reaction parameter, more atoms move, which are more likely to collide with the reactant particles, causing the reaction to occur faster and reflecting the strengthened interfacial mass transfer by a chemical reaction.

3.6. Effect of variation of different parameters on Sherwood number coefficients

The effect of the Schmidt number (S_c) on the Sherwood number is given in Tab. 9.The Sherwood number (Sh) increased with increasing Schmidt number (S_c). Tab. 10 reflects the effect of the Soret number on the Sherwood number. Here it is noticed that the Sherwood number increases with increased Soret number (S_o). Tab. 11 shows the behaviour of the chemical reaction parameter with respect to the Sherwood number. Clearly, the Sherwood number is a decaying function of the chemical reaction parameter (Kr). ($R = 5$ taken as constant).

Tab. 9. Variation with Schmidt number

S_c	Du	S_o	Ec	M^2	K	Gr	Gc	Pr	Q	Kr	Sh
0.71	4	6	0.04	3	0.5	5	6	0.82	1	5	1.5742
0.72	4	6	0.04	3	0.5	5	6	0.82	1	5	1.5886
0.73	4	6	0.04	3	0.5	5	6	0.82	1	5	1.6029
0.74	4	6	0.04	3	0.5	5	6	0.82	1	5	1.6170

Tab. 10. Variation with Soret number

S_o	Du	S_c	Ec	M^2	K	Gr	Gc	Pr	Q	Kr	Sh
5	4	0.71	0.04	3	0.5	5	6	0.82	1	5	1.3136
6	4	0.71	0.04	3	0.5	5	6	0.82	1	5	1.5742
7	4	0.71	0.04	3	0.5	5	6	0.82	1	5	1.7744
8	4	0.71	0.04	3	0.5	5	6	0.82	1	5	1.9401

Tab. 11. Variation with chemical reaction parameter

Kr	Du	S_o	Ec	M^2	S_c	K	Gr	Gc	Pr	Q	Sh
2	4	6	0.04	3	0.71	0.5	5	6	0.82	1	1.7754
4	4	6	0.04	3	0.71	0.5	5	6	0.82	1	1.6477
6	4	6	0.04	3	0.71	0.5	5	6	0.82	1	1.4918
8	4	6	0.04	3	0.71	0.5	5	6	0.82	1	0.9127

3.7. Comparison of the results

The results of present study are validated by comparing them with results of published studies in the absence of chemical reaction, viscous dissipation and Dufour effect, as obtained by Reddy et al. [23]. The same can be interpreted from Figs. 13 and 14.
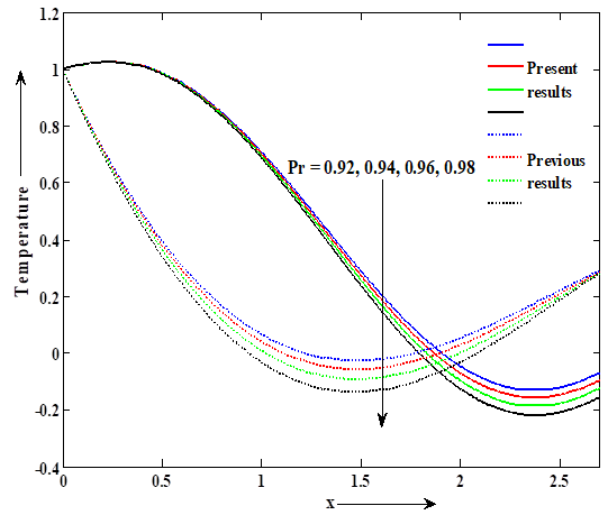

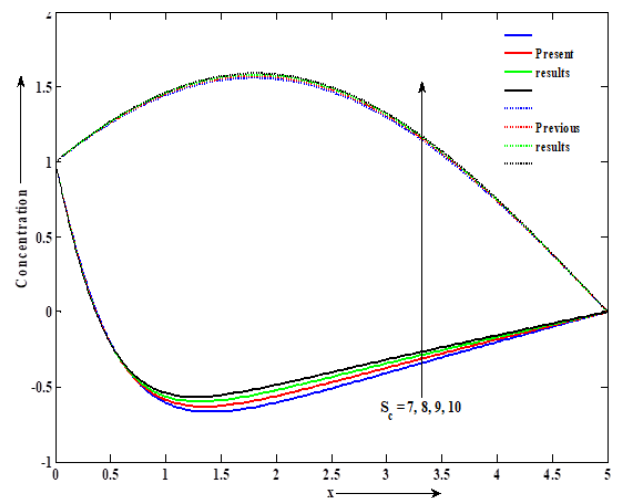**Fig. 13.** Comparison of the results. Effect of Pr on temperature in the absence of Du, Ec and Kr

Fig. 14. Comparison of the results. Effect of S_c on concentration in the absence of Du, Ec and Kr

Aastha Aastha, Khem Chand

DOI 10.2478/ama-2023-0030

Soret and Dufour Effects on Chemically Reacting and Viscous Dissipating Nanofluid Flowing Past a Moving Porous Plate in the Presence of a Heat Source/Sink

4. CLOSING REMARKS

In this study, the effect of viscous dissipation, heat source/sink, characteristics of heat and mass transfer on a chemically reacting magneto-nanofluid in a conducting field passing through a vertically moving porous plate in the presence of Soret and Dufour effects has been studied. By the using of the Laplace transform technique, Partial Differential Equations is converted to a set of Ordinary Differential Equations, and the numerical solutions are obtained by the MATLAB software package using the bvp4c function. From the numerical analysis, the following observations are derived:

− With an increase in the Grashof number and mass Grashof number, the velocity of the fluid is accelerated, while a reverse trend is observed in case of an increase in the magnetic parameter. In case of porosity parameter, velocity increases for the motion of the plate in forward direction, i.e., $\lambda = 1$, while the reverse trend is observed for the motion in backward direction, i.e., $\lambda = -1$.

− Temperature of the fluid is inversely related to the Eckert number, Prandtl number and heat source/sink parameter, whereas the Dufour number is directly related to it.

− The concentration profile declines with an increase in the Schmidt number, while it increases with an increase in the Soret number and chemical reaction parameter.

− An increase in the magnetic parameter leads to an increase in the skin friction coefficient, while an opposite effect is observed in case of Grashof number, mass Grashof number and porosity parameter.

− The local Nusselt number is enhanced with enhancement in the heat source/sink parameter, Eckert number and Prandtl number, but a reverse effect is observed in case of Dufour number.

− The Sherwood number increases with increasing Schmidt number and Soret number, whereas it decreases for the chemical reaction parameter.

− A comparison of results with those of previous studies validate the findings of the current study.

− In particular, the flow profile variations with respect to viscous dissipation, heat source/sink and chemical reaction in combination with Soret and Dufour effects have a great significance; thus, they find application in many engineering and industrial fields, particularly in separation of isotopes.

− The current study reveals that in the presence of chemical reaction, the mass transfer rate increase, causing the reaction to occur faster and also the viscous dissipation effect increases the heat transfer rate.

REFERENCES

1. Gupta M, Singh V, Kumar R, Said Z. A review on thermophysical properties of nanofluids and heat transfer applications. Review Sust Energy Rev. 2021; 74: 638-670. https://doi.org/10.1016/j.rser

2. Turkyilmazoglu M, Pop I. Heat and mass transfer of unsteady natural convection flow of some nanofluids past a vertical infinite flat plate with radiation effect. International Journal of Heat and Mass Transfer. 2013; 59:pp. 167171.

3. Dalir N, Nourazar S S. Solution of the boundary layer flow of various nanofluids over a moving semi-infinite plate using HPM. Mechanika. 2014; 20: pp. 57-63.

4. Ghalambaz M, Noghrehabadi A, Ghanbarzadeh A. Natural convection of nanofluids over a convectively heated vertical plate embedded in a porous medium. Brazilian Journal of Chemical Engineering. 2014; 31: 413-427.

5. Sulochana C, Samrat SP. Unsteady MHD Radiative flow of a Nano liquid past a permeable stretching sheet: An analytical study. Journal of Nanofluids. 2017; vol. 6: pp. 711-719.

6. Mishra A, Sharma BK. MHD Mixed Convection Flow in a Rotating Channel in the Presence of an Inclined Magnetic Field with the Hall Effect. Journal of Engineering Physics and Thermophysics 90, 2017; 1488–1499. https://doi.org/10.1007/s10891-017-1710-y

7. Ashwinkumar GP , Sulochana C, Samrat SP .Effect of the aligned magnetic field on the boundary layer analysis of magnetic-nanofluid over a semi-infinite vertical plate with ferrous nanoparticles. Multidiscipline Modeling in Materials and Structures. 2018; Vol. 14 No. 3: pp. 497-515. https://doi.org/10.1108/MMMS-10-2017-0128

8. Samrat SP, Sulochana, C, Ashwinkumar GP. Impact of Thermal Radiation on an Unsteady Casson Nanofluid Flow Over a Stretching Surface. International Journal of Applied and Computational Mathematics 5. 2019; 31. https://doi.org/10.1007/s40819-019-0606-2

9. Shaw S, Motsa, SS, Sibanda P. Nanofluid flow over three different geometries under viscous dissipation and thermal radiation using the local linearization method. Heat Transfer-Asian Research, 2019; 48(3). doi:10.1002/htj.21497

10. Kumar MA, Reddy YD, Goud BS, Rao VS. Effects of Soret, Dufour, hall current and rotation on MHD natural convective heat and mass transfer flow past an accelerated vertical plate through a porous medium. International Journal of Thermofluids. 2021; volume9: 100061.

11. Khan SA, Hayat T, Alsaedi A, Ahmad B. Melting heat transportation in radiative flow of nanomaterials with irreversibility analysis. Renewable and Sustainable Energy Reviews. 2021; Volume 140: 110739 ISSN 1364-0321, https://doi.org/10.1016/j.rser.2021.110739

12. Rasheed HUR, Islam S, Khan Z, Alharbi SO, Alotaibi H, Khan I. Impact of Nanofluid flow over an elongated moving surface with a uniform Hydromagnetic field and non-linear Heat reservoir. Hindawi Complexity. 2021; volume 2021: Article ID9951162.

13. Kumawat C, Sharma BK, M Al-Mdallal Q, Rahimi-Gorji M. Entropy generation for MHD two phase blood flow through a curved permeable artery having variable viscosity with heat and mass transfer. International Communications in Heat and Mass Transfer. 2022; Volume 133: 105954, ISSN 0735-1933. https://doi.org/10.1016/j.icheatmasstransfer.2022.105954

14. Tlili I, Baleanu D, Mohammad Sajadi S, Ghami F, Fagiry MA. Numerical and experimental analysis of temperature distribution and melt flow in fiber laser welding of Inconel 625. The International Journal of Advanced Manufacturing Technology. 2022; 121: 765–784. https://doi.org/10.1007/s00170-022-09329-3

15. Hejazi HA, Ijaz Khan M, Raza A, Smida K, Khan SU and Tlili I. Inclined surface slip flow of nanoparticles with subject to mixed convection phenomenon: Fractional calculus applications. Journal of the Indian Chemical Society, 2022; Volume 99: Issue 7, 100564, ISSN 0019-4522. https://doi.org/10.1016/j.jics.2022.100564

16. Anantha Kumar K, Sandeep N, Samrat SP, Ashwinkumar GP. Effect of electromagnetic induction on the heat transmission in engine oil-based hybrid nano and ferrofluids: A nanotechnology application. Proceedings of the Institution of Mechanical Engineers, Part E: Journal of Process Mechanical Engineering. 2022;0(0). doi:10.1177/09544089221139569

17. Veera Krishna M. Numerical investigation on steady natural convective flow past a perpendicular wavy surface with heat absorption/generation. International Communications in Heat and Mass Transfer. 2022; Volume 139: 106517, ISSN 0735-1933. https://doi.org/10.1016/j.icheatmasstransfer.2022.10657

18. Khanduri U, Sharma BK. Hall and ion slip effects on hybrid nanoparticles (Au-GO/blood) flow through a catheterized stenosed artery with thrombosis. Proceedings of the Institution of Mechanical Engineers, Part C: Journal of Mechanical Engineering Science. 2022;0(0). doi:10.1177/09544062221136710

19. Sharma BK, Gandhi R, Mishra NK, Al-Mdallal QM. Entropy generation minimization of higher-order endothermic/exothermic chemical reaction with activation energy on MHD mixed convective flow over a stretching surface. Scientific Reports 12. 2022; 17688.
https://doi.org/10.1038/s41598-022-22521-5

20. Khanduri U, Sharma BK. Entropy Analysis for MHD Flow Subject to Temperature-Dependent Viscosity and Thermal Conductivity. In: Banerjee, S., Saha, A. (eds) Nonlinear Dynamics and Applications. Springer Proceedings in Complexity. Springer, Cham. 2022.
https://doi.org/10.1007/978-3-030-99792-2_38

21. Cramer KR, Pai SI. Magnetofluid Dynamics for Engineers and Applied Physicists. McGraw-Hill, New York, 1973.

22. Das S, Jana RN. Natural convective magnetonanofluid flow and radiative heat transfer past a moving vertical plate. Alexandria Engineering Journal. 2015; 54:55–64.

23. Reddy PC, Raju MC, Raju GSS. Free Convective Heat and Mass Transfer Flow of Heat-Generating Nanofluid past a vertical moving porous plate in a Conducting field. Special Topics & Reviews in Porous Media – An International Journal. 2016;7(2): 161-180.
10.1615/SpecialTopicsRevPorousMedia.2016016973

Nomenclature

u' = Velocity component along the coordinate axis (m sec^{-1})

T' = Temperature (K)

T'_∞ = Ambient temperature (K)

T'_w = Temperature at the plate (K)

C' = Concentration (kg m^{-3})

C'_∞ = Ambient species concentration (kg m^{-3})

C'_w = Concentration at the plate (kg m^{-3})

t' = Time (sec)

$\overrightarrow{B_O}$ = Magnetic field (Tesla)

C_p = Specific heat at constant pressure $(J\,K^{-1}\text{kg}^{-1})$

ρ_{nf} = Density of the nanofluid (kg m^{-3})

μ_{nf} = Dynamic viscosity of the nanofluid (Pa s)

$(\rho C_p)_{nf}$ = Heat capacitance of the nanofluid $(J\,K^{-1})$

k_{nf} = Thermal conductivity of the nanofluid (W $m^{-1}K^{-1}$)

σ_{nf} = Electrical conductivity of the nanofluid $(\text{ohm}^{-1}\text{s}^{-1})$

ρ_f = Density of the base fluid (kg m^{-3})

ρ_s = Density of the nanoparticles (kg m^{-3})

σ_f = Electrical conductivity of the base fluid $(\text{ohm}^{-1}\text{s}^{-1})$

σ_s = Electrical conductivity of the nanoparticles $(\text{ohm}^{-1}\text{s}^{-1})$

μ_f = Viscosity of the base fluid nanoparticles (Pa s)

D = Mass diffusion coefficient $(m^2\,sec^{-1})$

D_1 = Thermal diffusion coefficient $(\text{m}^2\,sec^{-1})$

g = Acceleration due to gravity (m sec^{-2})

ϕ = Solid volume fraction of the nanoparticles (m g)

β_{nf} = Thermal expansion coefficient (K^{-1})

β'_{nf} = Mass transfer coefficient (m sec^{-1})

x' = Cartesian coordinate (m)

K'_p = Porosity medium permeability coefficient

q_o = Dimensional heat generation/absorption coefficient

K_1 = Chemical reaction rate

Superscript

´   Dimensional

Non-dimensional parameters

$Gr = \frac{g\beta\mu_f(T'_w - T'_\infty)}{u_0^3}$ (Grashof number)

$Gc = \frac{g\beta_f\mu_f(C'_w - C'_\infty)}{u_0^3}$ (modified Grashof number)

$M^2 = \frac{\sigma_f B_o^2 v_f}{\rho_f u_o^2}$ (magnetic parameter)

$K = \frac{K'_p u_0^2}{v_f^2}$ (porosity parameter)

$Pr = \frac{\mu_f C_p}{k_f}$ (Prandtl number)

$Ec = \frac{u_0^2}{C_p(T'_w - T'_\infty)}$ (Eckert number)

$Du = \frac{D}{v_f}\left(\frac{C'_w - C'_\infty}{T'_w - T'_\infty}\right)$ (Dufour number)

$S_c = \frac{v_f}{D}$ (Schmidt number)

$S_o = \frac{D_1}{v_f}\left(\frac{T'_w - T'_\infty}{C'_w - C'_\infty}\right)$ (Soret number)

$S_c = \frac{v_f}{D}$ (Schmidt number)

$Kr = \frac{K_1 v_f}{u_0^2}$ (chemical reaction parameter)

$Q = \frac{q_0 v_f^2}{k_f u_0^2}$ (heat source/sink parameter)

Appendix

Code for the numerical method: -
For differential equations:

```
global  D  s  W  C  E  M  A  K  G  B  F  A5  P  R  n  Q
T
 dydx= [y (2)
       C*W*E*P*(y (5) ^2) +C*W*P*((n/P)
*Q-s)  *y(1)-C*(s-T)  *y(3)/(1-C*W*D*P)
       y (4)
       P*((-D*C*W*E*P*(y (6) ^2)
+D*C*W*P*(n/P*Q-s)  *y(1)-D*C*(s-T)
*y(3)/(1-C*W*D*P))-E*(y (6) ^2) -((n/P)
*Q-s)  *y (1))
       y (6)
       (s+(M^2) *A+1/K) *y (5)-G*B*y
(1)-
F*A5*y (3)];
```

For boundary conditions:

```
global L
res= [ya (1)-1
     ya (3)-1
     ya (5)-L
     yb (1)
     yb (3)
     yb (5)];
```

Aastha Aastha: https://orcid.org/0000-0002-1175-361X

Khem Chand: https://orcid.org/0000-0002-6360-7729